ChemPubSoc Europe

DOI: 10.1002/open.201700154

Open Access ChemistryOPEN Full Papers

Rhodol Derivatives as Selective Fluorescent Probes for the Detection of Hg^{II} Ions and the Bioimaging of Hypochlorous Acid

Ling Li,[a] Shu Wang,[a] Hongxia Lan,[b] Guiyi Gong,[b] Yifan Zhu,[a] Yu Chung Tse,*[b] and Keith Man-Chung Wong*[a]

Two sensors, **1** with a spirolactone group and **2** with a spirolactam group containing a phenyl isothiocyanate moiety, based on rhodol, were designed and synthesized in order to obtain materials with excellent optical properties for the detection of environmentally and biologically important Hg^{2+} and hypochlorous acid (HClO) ions. The crystal structure of **1** revealed two moieties, a rhodamine-like portion with a spirolactone and a fluorescein-like portion without a spirolactone. In the absence of analyte, **1** produced an optical output with a maximum absorption and emission at 475 and 570 nm, respectively, which was attributed to the fluorescein-like moiety without a spirolactone. In contrast, the rhodamine-like moiety containing a spirolactone was activated by the addition of H^+ or Hg^{2+} ions, and **1** yielded new absorption and emission peaks at 530 and 612 nm, respectively. Further functionalization with a phenyl isothiocyanate group afforded **2**, a fluorescent probe for HClO. High selectivity and sensitivity towards the hypochlorite ion were anticipated, owing to the stoichiometric and irreversible formation of a thiosemicarbazide group, which led to dramatic fluorescence responses. With good functionality at physiological pH, probe **2** was successfully used to image HClO in HeLa cells.

1. Introduction

All living systems use metal cations, inorganic anions, and small-molecule gases for biological functions. These chemical species all interact with biological macromolecules, thus driving a multitude of structural and catalytic processes. The numerous applications of this research area include signal detection for a variety of metal ions and inorganic species that trigger pathology and drive physiological processes.

The divalent mercury cation, Hg^{II}, one of the most dangerous and widespread global pollutants, has high affinity for the thiol groups in proteins, and this interaction leads to cell malfunction and consequently causes many health problems in the brain, kidney, and central nervous system. Hg^{II} accumulation in the body results in a wide variety of diseases, such as prenatal brain damage, severe cognitive and motion disorders, and Minamata disease. Therefore, developing a convenient and rapid method for the determination of mercury in biological and environmental samples is urgently needed.[1] Owing to the simplicity and high sensitivity of fluorescence detection, fluorescent probes are regarded as the most powerful tools for biologically monitoring metal ions in vitro and/or in vivo.[2] Utilization of rhodamine derivatives as fluorescent chemosensors for mercury ions have been extensively studied in the past decade.[3]

Similarly to mercury, hypochlorous acid (HClO), a reactive oxygen species (ROS), plays an essential role in immune defense against microorganisms and inflammation. However, excessive HClO formation can lead to severe diseases including cancer, neurodegenerative disorders, and cardiovascular diseases.[4,5] Therefore, the detection of HClO in living cells has become a popular area in biological and chemical research. Several methods, including electroanalysis,[6] potentiometry,[7] spectrophotometry,[8] chemiluminescence,[9] and fluorescence[10,11] methods, have been reported for the analysis of HClO. Among these techniques, small-molecular fluorescent probes are attractive, because they create less cell damage and respond in a selective manner to specific analytes.[10–12]

This important research motivated us to construct sensitive probes for detecting Hg^{2+} and HClO. This detection ability would have the potential to greatly improve biochemical techniques that detect these analytes in live cells and tissues.[13]

[a] L. Li, S. Wang, Y. Zhu, Prof. K. M.-C. Wong
Department of Chemistry
Southern University of Science and Technology
No. 1088, Tangchang Boulevard
Nanshan District, Shenzhen 518055 (P.R. China)
E-mail: keithwongmc@sustc.edu.cn

[b] Dr. H. Lan, G. Gong, Prof. Y. C. Tse
Guangdong Provincial Key Laboratory of Cell Microenvironment and Disease Research, Shenzhen Key Laboratory of Cell Microenvironment
Department of Biology, Southern University of Science and Technology
No. 1088, Tangchang Boulevard
Nanshan District, Shenzhen 518055 (P.R. China)
E-mail: tseyc@sustc.edu.cn

Supporting Information and the ORCID identification number(s) for the author(s) of this article can be found under https://doi.org/10.1002/open.201700154.

Among the fluorescent probes, an interesting class of rhodamine-based probes with two spirocyclic rings for detecting Hg^{2+} has been reported by us.[14] On the other hand, another fluorescent dye, rhodol, possessing the merits of its structural parent units, rhodamine and fluorescein, as well as being rather less pH dependent, has received considerable attention.[15] As an extension of our group's previous work on novel rhodamine derivatives[16] and their combination with transition-metal complexes,[17] we herein report the synthesis as well as the photophysical and chemical properties of rhodol derivative **1** that contains only one spirolactone group. The results suggested that probe **1** exhibits an impressively high selectivity towards Hg^{2+} over other metal ions. In addition, a HClO-selective fluorescent probe **2** was prepared by modification with a phenyl isothiocyanate group, and it undergoes an irreversible HClO-promoted reaction. The new probe **2** exhibited good sensitivity and selectivity for HClO over other ROS and/or reactive nitrogen species (RNS) in phosphate-buffered saline (PBS) buffer. Moreover, probe **2** can be used for bioimaging endogenous HClO within HeLa cells.

Experimental Section

Materials and Reagents

Hydrazine hydrate (98%), benzaldehyde (98%), and methanesulfonic acid (99%) were purchased from Energy Chemical. 3-(Diethylamino)phenol (97%, Sigma–Aldrich Chemical Co.), phthalic anhydride (Tianjin Fuchen Chemical Reagents Factory), 2-methylresorcinol (98%, J&K Scientific Ltd.), isothiocyanato benzene (Adamas), sodium hypochlorite (Tianjin Fuyu Chemical Reagents Factory), and other materials for the synthesis were used without further purification. All chemicals used for the synthesis were of analytical grade. Methanol for analysis was of spectroscopy grade. Copper(II) perchlorate, sodium(I) perchlorate, lead(II) perchlorate trihydrate, cadmium(II) perchlorate hexahydrate, lithium(I) perchlorate, magnesium(II) perchlorate, cobalt(II) perchlorate, and iron(II) perchlorate hydrate were of reagent grade (RG) and were purchased from Alfa Aesar. Zinc(II) perchlorate hexahydrate (RG, Aladdin Chemical Co., Ltd.), barium(II) perchlorate (RG, Sigma–Aldrich Chemical Co.), and silver(I) perchlorate (analytical grade (AR), Energy Chemical) were obtained from the indicated vendors, and nickel(II) perchlorate hexahydrate and mercury(II) perchlorate trihydrate with purities above 99.0% were purchased from Strem Chemicals, Inc.

Instrumentation

Absorption spectra were recorded with a Cary 60 UV/Vis absorption spectrophotometer. Fluorescence spectra were recorded with an FLS 980 fluorescence spectrometer from Edinburgh Instrument TM at room temperature. Quartz cuvettes (path length = 1 cm) were used for all spectrophotometric and fluorometric measurements. Nuclear magnetic resonance (NMR) spectra were recorded with a Bruker AVANCE 400 spectrometer (400 MHz for ^{1}H NMR and 101 MHz for ^{13}C NMR). Fourier transform NMR spectrometry was used to determine chemical shifts relative to chloroform or methanol. Low-resolution and high-resolution mass spectrometry (HRMS) data were obtained with an Orbitrap Fusion TM Tribrid TM mass spectrometer.

Synthesis

Synthesis of S1

S1 was prepared according to the reported procedures.[14]

Synthesis of S2

A solution of benzaldehyde (1.06 g, 10 mmol) and 2-methylresorcinol (2.48 g, 20 mmol) in $MeSO_3H$ (50 mL) was heated at 70 °C for 24 h, and a dark solution was produced. The reaction mixture was cooled to room temperature and poured into 400 mL of an aqueous solution of 3 M NaOAc. The resulting dark-red solid was collected by filtration to provide the crude product. The product was purified by column chromatography on silica gel with dichloromethane/methanol (40:1, v/v), thus yielding a red–brown intermediate **S2** (1.32 g, 41%)

Characterization Data for S2

^{1}H NMR (400 MHz, CD_3OD) δ 7.62 (d, J = 3.4 Hz, 3H), 7.45–7.37 (m, 2H), 6.91 (d, J = 9.2 Hz, 2H), 2.09 (s, 6H,).

Synthesis of Compound 1

Concentrated sulfuric acid (6 mL) was added dropwise to a mixture of **S1** (0.25 g, 0.8 mmol) and **S2** (0.25 g, 0.8 mmol) at 0 °C. The resulting suspension was heated to 100 °C and maintained for 3 h. After the mixture was cooled to room temperature and poured into ice water (20 mL) with vigorous stirring, the pH of the mixture was adjusted to approximately 7. The mixture was extracted with dichloromethane (20 mL) three times. The organic layers were dried with anhydrous magnesium sulfate and evaporated to yield the crude product. The product was purified and separated by silica column chromatography, with elution with dichloromethane/methanol (50:1), thus yielding the pure form of **1** (0.24 g, 51%)

Characterization Data for 1

^{1}H NMR (400 MHz, $CDCl_3$) δ 7.85–7.83 (d, J = 7.8 Hz, 1H), 7.64–7.60 (t, J = 7.5 Hz, 1H), 7.55–7.51 (t, J = 7.5 Hz, 1H), 7.44–7.34 (m, 2H), 7.20–7.17 (m, 2H), 7.14–7.12 (d, J = 7.6 Hz, 1H), 7.04–7.02 (d, J = 9.8 Hz, 1H), 6.90–6.88 (m, 1H), 6.60–6.56 (m, 3H), 6.40–6.37 (d, J = 11.5 Hz, 2H), 3.42–3.37 (q, J = 7.1 Hz, 4H), 2.69 (s, 3H), 2.28 (s, 3H), 1.22–1.18 (t, J = 7.1 Hz, 6H). ^{13}C NMR (101 MHz, $CDCl_3$) δ 185.39, 169.12, 154.45, 153.47, 153.04, 152.35, 151.70, 151.25, 150.09, 149.85, 147.08, 134.74, 132.52, 129.91, 129.67, 129.33, 128.95, 128.82, 128.07, 127.29, 126.10, 124.95, 123.84, 119.18, 117.11, 116.72, 114.52, 113.52, 109.10, 108.62, 105.52, 104.67, 98.06, 83.78, 44.66, 12.68, 8.70, 8.19. HRMS (electrospray ionization (ESI)) for $C_{39}H_{32}NO_5$ $[M+H]^+$: calcd 594.22750; found: 594.22702.

Synthesis of S3

Hydrazine (5 mL) was added to a suspension of **1** (300 mg, 0.5 mmol) in ethanol (20 mL). The resulting suspension was refluxed overnight. After the resulting suspension was cooled to room temperature, deionized water (20 mL) was added to the residue. The aqueous phase was extracted with dichloromethane (20 mL) three times. The organic phase was dried by anhydrous magnesium sulfate. The solvent was removed to yield the crude product of **S3** (260 mg, 87%). The purification and separation of

the stereoisomer were achieved by silica column chromatography, with elution with dichloromethane/methanol (50:1), thus yielding the pure form of **S3** as an orange solid after solvent removal.

Characterization Data for S3

^{1}H NMR (400 MHz, $CDCl_3$) δ 7.83–7.76 (d, J=6.5 Hz, 1H), 7.51–7.33 (m, 4H), 7.17 (dt, J=7.9, 4.1 Hz, 2H), 7.09–6.97 (m, 2H), 6.83 (d, J=7.7 Hz, 1H), 6.60–6.51 (m, 2H), 6.47–6.39 (m, 1H), 6.39–6.30 (m, 2H), 3.71–3.60 (m, 2H), 3.34–3.39 (q, J=6.7 Hz, 4H), 2.68 (s, 3H), 2.26 (s, 3H), 1.19 (t, J=7.0 Hz, 6H).

Synthesis of Compound 2

A mixture of **S3** (200 mg, 0.3 mmol) and phenyl isothiocyanate (180 µL, 1.48 mmol) in dimethylformamide (DMF, 2 mL) was stirred at room temperature for 24 h under nitrogen. The solvent was removed, and the crude product was purified by silica column chromatography, with elution with hexane/ethyl acetate (1:1), thus yielding the crude product as an orange solid after solvent removal. Subsequent recrystallization of the compound by diffusion of diethyl ether vapor into a solution of the crude product in dichloromethane afforded pure **2** (99 mg, 49.5%).

Characterization Data for 2

^{1}H NMR (400 MHz, $CDCl_3$) δ 7.87–7.85 (d, J=7.6 Hz, 1H), 7.67–7.63 (t, J=7.6, 1.3 Hz, 1H), 7.58–7.54 (t, J=7.5, 1.0 Hz, 1H), 7.36–7.35 (m, 2H), 7.23–7.18 (d, J=7.6 Hz, 1H), 7.17–7.09 (m, J=16.1, 8.2 Hz, 3H), 7.0–6.81 (m, J=7.4 Hz, 4H), 6.82–6.80 (d,1H), 6.58–6.54 (m, 3H), 6.37–6.34 (dd, J=8.9, 2.6 Hz, 1H), 6.25 (s, 1H), 3.4–3.34 (q, J=7.1 Hz, 4H), 2.66 (s, 3H), 2.25 (s, 3H), 1.20–1.16 (t, J=7.0 Hz, 6H). ^{13}C NMR (101 MHz, $CDCl_3$) δ 185.21, 182.35, 166.31, 154.10, 153.97, 151.45, 149.83, 148.79, 146.21, 137.35, 134.28, 132.15, 129.66, 129.57, 129.24, 128.79, 127.93, 127.70, 126.06, 124.87, 124.79, 128.34, 127.93, 127.70, 126.06, 124.87, 124.30, 124.16, 123.97, 119.15, 117.04, 115.55, 114.45, 114.07, 109.46, 102.95, 98.54, 77.21, 66.66, 44.46, 29.70, 12.53, 8.67, 8.03. HRMS: m/z $[M+H]^+$ calcd for $C_{46}H_{39}N_4O_4S$: 743.26865; found: 743.26859.

Buffers of Different pH

Different buffer solutions were prepared with 50 mM potassium hydrogen phthalate (for pH 1–5 buffers), 25 mM potassium dihydrogen phosphate (for pH 6–8 buffers), 10 mM sodium tetraborate (for pH 9–10 buffers), and 50 mM sodium bicarbonate (for pH 11–14 buffers). The pH was adjusted by addition of 0.1 M NaOH or 0.1 M HCl solutions.

Biological Imaging

HeLa cells were seeded in glass-bottom cell culture dishes and cultured in DMEM with 10% fetal bovine serum, 1% penicillin-streptomycin (10000 IU penicillin m^{-}; 10000 µg streptomycin m^{-}) at 37 °C in a humidified 5% CO_2/95% air incubator. After 16–24 h, the HeLa cells were washed and treated with or without 50 mM NaClO in DMEM medium for 1 h. Then, the cells were washed three times before incubation with or without 12.5 µM probe **2** in DMEM containing 1% DMSO for 2 hours. After incubation, the cells were washed with PBS buffer and then subjected to fluorescence confocal microscopy imaging (Leica SP8, Germany). The 16-bit images were collected, and the normalized fluorescence intensity (threshold valve, 8000) was analyzed by using ImageJ software.

2. Results and Discussion

2.1. Synthesis and Characterization

The synthetic route for probe **1** is outlined in Scheme 1. Aldol condensation of benzaldehyde and 2-methylresorcinol in $MeSO_3H$ yielded compound **S2**. Then, product **1** was obtained

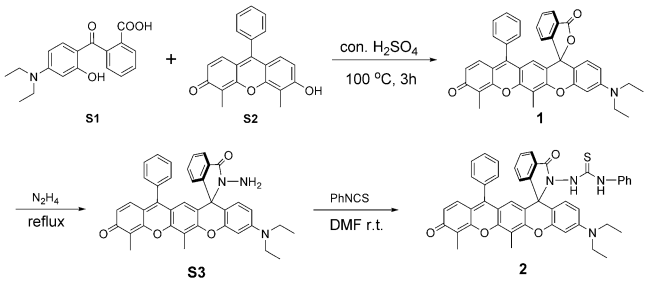

Scheme 1. Synthetic route for **1** and **2**.

by the reaction of **S1**[4a] and **S2** in concentrated sulfuric acid under reflux conditions. The structure of **1** was determined by X-ray crystallography (Figure 1), and all of the experimental details are given in Table 1. In addition, selected bonds (Å) and angles (°) are listed in Table S1. The O1–C30 distance of 1.247 Å is shorter than the C–O distance of a phenolic hydroxyl group of approximately 1.43 Å. Moreover, the C31–C32 and C28–C29 distances were 1.344 and 1.340 Å, respectively, which are slightly shorter than the C–C bond distance in the benzene ring of approximately 1.395 Å. This result indicated that the structure of probe **1** includes a ketone group. The dihedral angle O4–C11–O3–C20 between the xanthene plane and spirolactone ring plane was 92.8°, which is close to a right angle. Therefore, similarly to the related compound named **control**,[16]

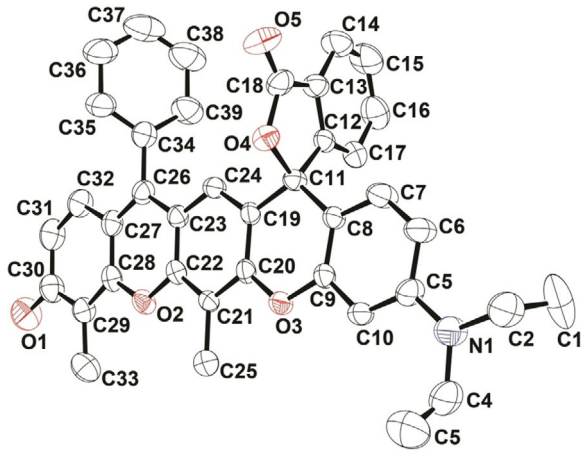

Figure 1. Perspective drawing of **1** with atomic numbering scheme. Hydrogen atoms and solvent molecules are omitted for clarity. Thermal ellipsoids are drawn at the 35% probability level.

Table 1. Crystal data and structure determination data for compound **1**.

Empirical formula	$C_{39}H_{31}O_5$	
Formula weight	593.65	
Temperature	293(2) K	
Wavelength	0.71073 Å	
Crystal system	monoclinic	
Space group	$P2_1/c$	
Unit cell dimensions	$a = 9.6361(9)$ Å	$\gamma = 90°$
	$b = 12.2079(11)$ Å	$\beta = 101.818(4)°$
	$c = 26.6548(19)$ Å	$\gamma = 90°$
Volume	3069.1(5) Å^3	
Z	4	
Density (calculated)	1.285 mg m^{-3}	
Absorption coefficient	0.085 mm^{-1}	
$F(000)$	1248	
Crystal size	0.278×0.231×0.059 mm^3	
Theta range for data collection	2.958 to 24.998°.	
Index ranges	$-11 \le h \le 11$, $-14 \le k \le 14$, $-31 \le l \le 31$	
Reflections collected	40224	
Independent reflections	5402 [R(int) = 0.2278]	
Completeness to theta = 24.998°	99.8 %	
Refinement method	full-matrix least-squares on F^2	
Data/ restraints/ parameters	5402/ 6/ 418	
Goodness-of-fit on F^2	1.020	
Final R indices [I > 2σ(I)]	$R1 = 0.0720$, $wR2 = 0.0881$	
R indices (all data)	$R1 = 0.2515$, $wR2 = 0.1210$	
Largest diff. peak and hole	0.148 and −0.172 e.Å^{-3}	

the fluorescent probe **1** for Hg^{2+} contains a xanthene moiety with a ketone group and a spirolactone ring on the amino side. The structural difference between **control** and **1** is the two methyl groups in the xanthene moiety of **1**, which cause its structure to be linear. The structure of **1** was well characterized by using standard spectroscopic techniques ^{1}H NMR, ^{13}C NMR and HRMS (Figures S1–S4). Probe **2** was readily prepared from probe **1** in a two-step reaction. The reaction of probe **1** with hydrazine yielded **S3**, which was then converted to the designed product **2** by further reaction with phenyl isothiocyanate (Scheme 1). The structure of probe **2** was confirmed by ^{1}H NMR, ^{13}C NMR and HRMS (Figures S5–S7).

2.2. Fluorescence Sensor for Hg^{2+}

The spirolactone ring of probe **1** was opened only after the addition of Hg^{2+} among various transition-metal ions, and the electronic absorption and emission spectra of **1** and its corresponding opened form, **1** + Hg^{2+}, are shown in Figure 2. Such a spirolactone ring-opening process was probably induced by the electrostatic interaction with the O atom(s) of the COO^- group upon binding of Hg^{2+}.[4] As shown, the maximum absorption and emission peaks without any analyte were observed at 475 and 570 nm. After addition of Hg^{2+}, the new absorption and emission peaks appeared at 530 and 612 nm, respectively.

2.2.1. Selective Hg^{2+} Sensing

Considering the spectral changes owing to the presence of Hg^{2+}, the potential use of **1** as a molecular probe was explored. The spectrophotometric response of **1** (10 μM) in methanol solutions of various metal ions and later to the addition of Hg^{2+} are shown in Figure 3. Two-fold additions of the tested metal ions did not cause an apparent absorbance increase by **1** at 530 nm. Two-fold additions of Cu^{2+} and Fe^{2+} resulted in a slight increase in the absorbance of **1** at 530 nm. However, Cu^{2+} and Fe^{2+} resulted in an absorbance enhancement that was far below that of a two-fold addition of Hg^{2+} under the same conditions. After addition of Hg^{2+} (2 equiv) to a solution of **1** containing interfering metal ions (2 equiv), significant absorbance at 530 nm was observed. All of these observations indicated that **1** exhibits highly preferential binding to Hg^{2+} over other metal ions. The corresponding color changes of **1** (10 μM) in the presence of different metal ions

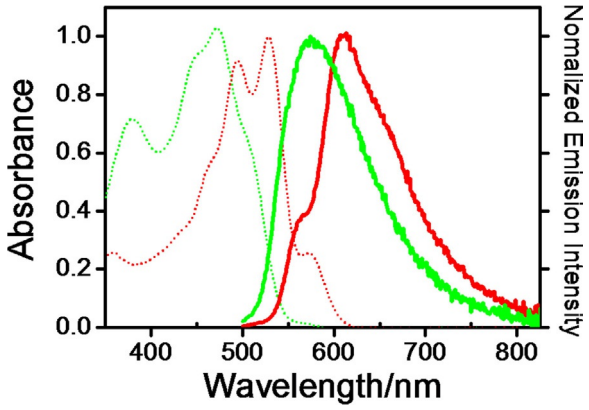

Figure 2. Electronic absorption (···) and emission (–) spectra of **1** (concentration = 2×10^{-5} M) in the absence (green lines) and presence (red lines) of Hg^{2+} in MeOH.

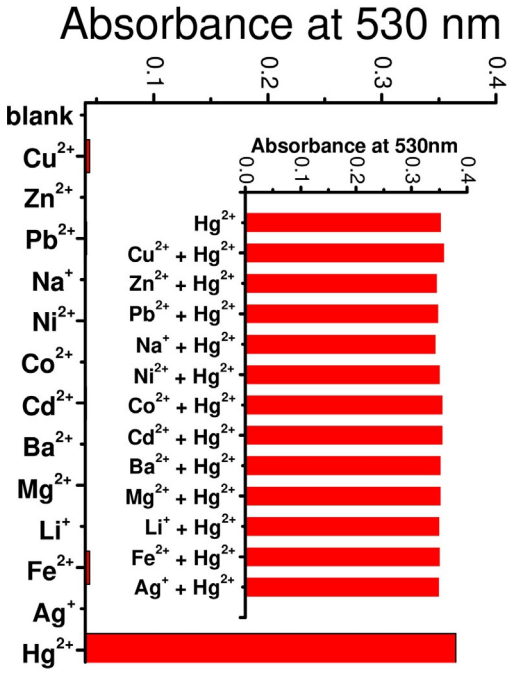

Figure 3. Selectivity study of **1** (conc. = 10^{-5} M) in MeOH upon addition of various metal ions (2 equiv) and interference of **1** (concentration = 10^{-5} M) in MeOH upon addition of Hg^{2+} and various metal ions.

Figure 4. Photograph of **1** (10^{-5} M in MeOH) showing the color change (upper) and emission enhancement at 365 nm (UV lamp) (down) in the presence of various metal ions (2 equiv). From left to right: blank, Cu^{2+}, Zn^{2+}, Pb^{2+}, Na^{+}, Ni^{2+}, Co^{2+}, Cd^{2+}, Ba^{2+}, Mg^{2+}, Li^{+}, Fe^{2+}, Ag^{+}, Hg^{2+}.

are illustrated in Figure 4. Among the metal ions investigated, mercury(II) induced a marked purple–red color change of **1**, whereas Cu^{2+}, Zn^{2+}, Pb^{2+}, Ni^{2+}, Co^{2+}, Cd^{2+}, Ba^{2+}, Mg^{2+}, Li^{+}, Fe^{2+} and Ag^{+} did not induce a color change of **1**. The prominent color change after the addition of Hg^{2+} to compound **1** allowed Hg^{2+} to be recognized by the naked eye.

2.2.2. Spectroscopic Titrations with Hg^{2+}

The absorption spectra of **1** after titration with Hg^{2+} are shown in Figure 5a. The yellow–green color of probe **1** in methanol was attributed to the moiety that resembles the opened spirolactone ring form of fluorescein, which consists of a benzene ring and a xanthene moiety with a ketone group. The addition of Hg^{2+} resulted in the emergence of a new absorption peak at 530 nm with shoulders at approximately 495 and 575 nm that increased gradually with the increase in Hg^{2+} concentration, thus indicating the formation of a delocalized xanthene moiety of **1** via ring opening of the spirolactam. Such growth of the absorption bands reached saturation at approximately 3 equivalents of Hg^{2+} addition. Moreover, the solution exhibited a marked and characteristic color change from yellow–green to purple–red, thus indicating that **1** serves as a "naked-eye" indicator of Hg^{2+}. At a total concentration of **1** and Hg^{2+} of 5×10^{-5} M, a Job plot was created from the absorbance at 575 nm, which exhibited maximum absorbance when the molecular fraction of **1** was 50%, suggesting a 1:1 binding stoichiometry between probe **1** and Hg^{2+} (Figure S8).

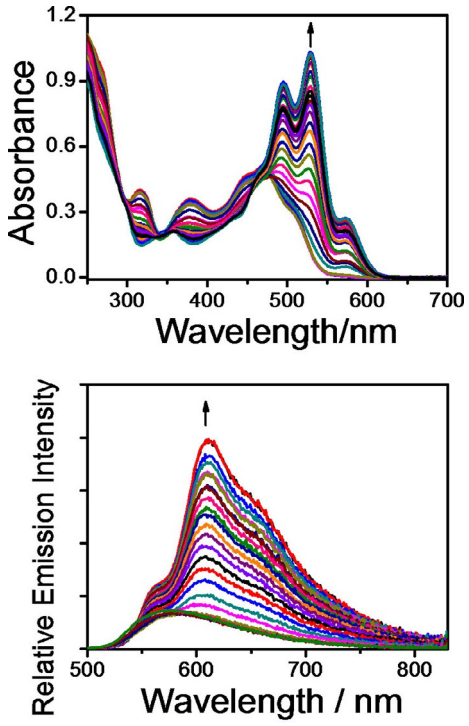

Figure 5. Electronic absorption (top) and emission (bottom) spectra of **1** (concentration = 2×10^{-5} M) in MeOH solution in the presence of various concentrations of Hg^{2+} (0–3 equiv). Ex. = 470 nm.

The fluorescence changes of probe **1** after the addition of Hg^{2+} were observed in a fluorescence titration experiment (Figure 5b). The solution of **1** showed weak fluorescence in the absence of analyte, owing to the fluorescein-like form. After addition of $Hg(ClO_4)_2$ to the methanol solution of **1**, a new emission band centered at 612 nm (with excitation at 470 nm) emerged. This absorbance at a longer wavelength dominated over the background signals caused by biological autofluorescence and other macromolecular compounds. The logK_s values for Hg^{2+} binding were 6.18 and 6.09, on the basis of the absorption and emission titration data, and the corresponding detection limits were calculated to be 8.6 and 7.6×10^{-6} M on the basis of the absorption and emission titration results, respectively (Figure S9).

After addition of H^{+}, probe **1** exhibited similar electronic absorption and emission spectral changes to those observed for Hg^{2+} addition (Figure S10), because of the formation of an extended π conjugation. Probe **1** was studied in MeOH–buffer solutions (1:1, v/v) with different pH values (pH 1.02–8) by using UV/Vis absorption spectroscopy (Figure S11), and the corresponding pK_a of **1** for the amino group was determined to be 3.1, a value similar to that of rhodamine.[18] The emission spectra of **1** in MeOH–buffer solutions of different pH values are also depicted in Figure S12. At basic–neutral pH, the maximum absorption and emission peaks of probe **1** were still located at 475 and 570 nm. In contrast, at acidic pH, probe **1** had maximal absorption at approximately 575 nm and maximal emission at approximately 612 nm, thus indicating its potential for use as a pH sensor.

The rhodamine derivatives with a phenylthiourea group are well documented to function as a Hg^{2+} chemodosimeter,[14] and it is anticipated that compound **2** possesses a similar sensing behavior. Corresponding electronic absorption and fluorescence titration studies of **2** with Hg^{2+} have been performed. Upon addition of Hg^{2+} into the solution of **2**, the electronic absorption spectra showed a new vibronic absorption bands at 500, 538, and 583 nm, whereas an emission band at 620 nm was observed in the emission spectra (Figure S13). Corresponding limits of detections were determined as 5.6 and 5.5×10^{-6} M from the absorption and emission spectral changes, respectively.

2.3. Fluorescence Sensor for HClO

2.3.1. Selective HClO Sensing

To test the selectivity for HClO, the emission spectra of probe **2** in PBS buffer (pH 7.45, containing 5% MeOH as a cosolvent) after separate addition of various ROS/RNS, including H_2O_2, NO_2^-, $ONOO^-$, OH^-, $^{\bullet}OH$, ClO_4^-, PO_4^{3-}, and ClO^-, were measured and are shown in Figure 6. A large and distinct enhancement of fluorescence intensity was observed only after the addition of HOCl, whereas negligible changes were observed for other analytes. These observations indicated the excellent selectivity of probe **2** towards HClO over other biologically relevant species under physiological conditions. Compound **1** without a phenylthiourea group was found to show negligible responses towards ClO^-.

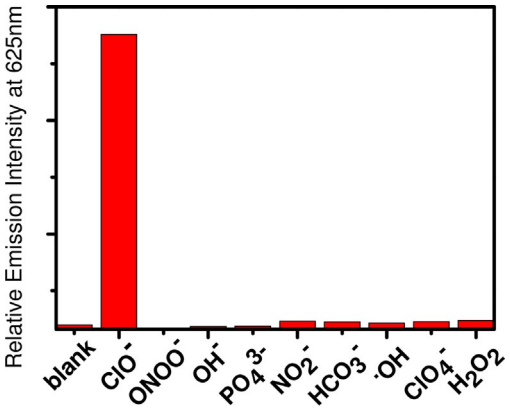

Figure 6. Fluorescence intensities at 625 nm when probe **2** (25 μM) was treated with NaClO (10 μM), H_2O_2 (200 μM), $^{\bullet}OH$ (100 μM Fe^{2+} + 1 mM H_2O_2), $ONOO^-$ (1 mM KNO_2 + 1 mM H_2O_2). OH^- (10 μM), HCO_3^- (10 μM), ClO_4^- (20 μM), NO_2^- (20 μM), and PO_4^{3-} (20 μM) in a PBS buffer (20 mM, pH 7.45, containing 5% MeOH as co-solvent) with excitation at 595 nm.

2.3.2. Spectroscopic Studies of 2

The changes in the absorption (Figure 7a) and fluorescence emission (Figure 7b) spectra of probe **2** in the absence and presence of HOCl in MeOH–PBS buffer solution (20 mM) (1:1, v/v pH 7.47) are shown. Probe **2** displayed absorption and weak emission bands at 475 and 570 nm, respectively, thus indicating that probe **2,** which is a further-functionalized probe **1**, also contains a fluorescein-like moiety. However, the addition of NaClO triggered a gradual decrease in the absorbance of the fluorescein-like group at 475 nm and the emergence and gradual increase in intensity of a new absorption band at 575 nm, thus suggesting that HClO induced the formation of 1,3,4-oxadiazole, as shown in Scheme 2. The results of emission titration studies showed an emergence of a new emission band at 612 nm over the former emission band at 570 nm. Moreover, the emission color of probe **2** dramatically changed from orange to purple–red after addition of NaClO. The corresponding detection limits were calculated to be 9.66 and 14×10^{-5} M on the basis of the absorption and emission titration results, respectively (Figure S14). The MS spectra indicated that

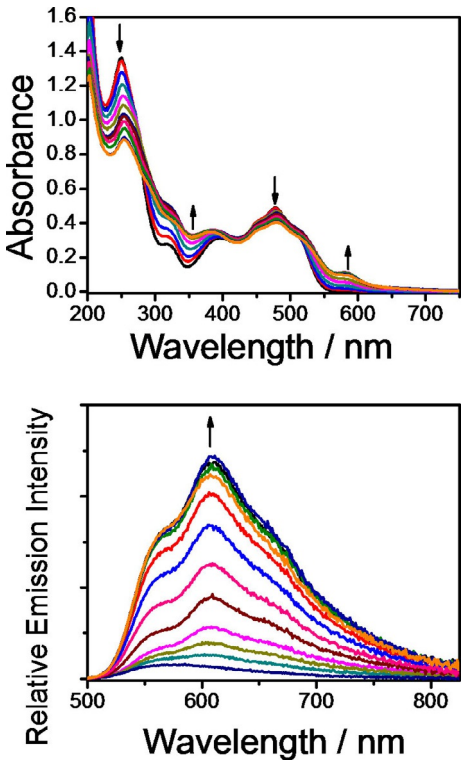

Figure 7. Electronic absorption (top) and emission (bottom) spectral changes (excitation = 487 nm) of **2** (concentration = 2.5×10^{-5} M) in MeOH/PBS buffer solution (20 mM) (1:1, v/v pH 7.47) in the presence of various concentrations of ClO^-.

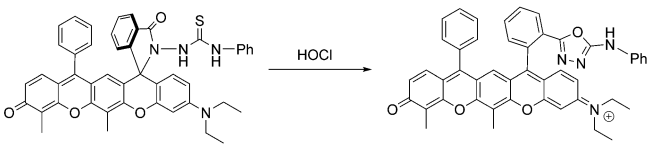

Scheme 2. HClO detection mechanism of **2**.

HClO reacts with probe **2** and forms a ring-opened rhodamine 1,3,4-oxadiazole (Figure S15), thus further supporting the fluorescence turn-on response. In addition, probe **2** was evaluated for its ability to detect HClO under near physiological conditions (20 mM PBS containing 5% MeOH as a co-solvent, pH 7.47) (Figure S16). The results indicated that the fluorescence sensor could be successfully applied in bioimaging.

2.3.3. Effect of pH

The effects of pH, a significant factor in the photophysical properties of a sensing probe, on the fluorescence response to HClO/ClO^- of probe **2** in the range of 4–10 were also studied, as shown in Figure S17. As expected, negligible fluorescence changes of **2** were observed at 612 nm with excitation at 595 nm during the pH variations. After the addition of NaClO, the fluorescence intensity of **2** in the presence of NaClO became significantly higher at pH 4–6. These results demonstrated that probe **2** exhibits high sensitivity towards HClO

rather than the hypochlorite ion (ClO^-), because the pK_a of HClO is 7.6.[19] Additionally, probe **2** can be used to detect HClO in living cells without interference from pH effects.

2.4. Biological Imaging

2.4.1. Exogenous Hypochlorite Ion Activates Probe 2 to Emit Fluorescence Signals in HeLa Cells

To examine whether probe **2** could function properly in biological samples, we incubated probe **2** with human cultured HeLa cells and imaged the samples by using fluorescence confocal microscopy. With excitation at 488 nm and emission at 500–750 nm as well as excitation at 552 nm and emission at 560–750 nm, autofluorescence was low in control HeLa cells (Figure 8A–D). In contrast, fluorescent puncta and diffuse fluorescence signals were observed in the cytoplasm of **2**-treated cells (Figure 8E–H). In addition, the fluorescence intensity in **2**-treated cells was significantly higher than in the control (Figure 8M,N). These data indicate that probe **2** is either permeable to the cell membrane or can be taken up by cells and subsequently emit fluorescent signals in human cells. Next, we determined whether exogenous ClO^- could activate probe **2** in living HeLa cells and lead to strong fluorescence emission. We treated HeLa cells with sodium hypochlorite (NaClO) before incubation with probe **2**. More fluorescent puncta and a higher fluorescence signals were observed in double-ClO^--**2**-HeLa cells than in the control (Figure 8I–L). In addition, fluorescence signals from filament-like structures and nuclei were observed in the sodium hypochlorite treatment (Figure 8I–L). Compared with that of the control, the overall intensity of double-ClO^--**2**-HeLa cells was approximately 2.5 times higher (Figure 8M,N). Collectively, these results suggested that probe **2** can effectively detect exogenous ClO^- in living human cells.

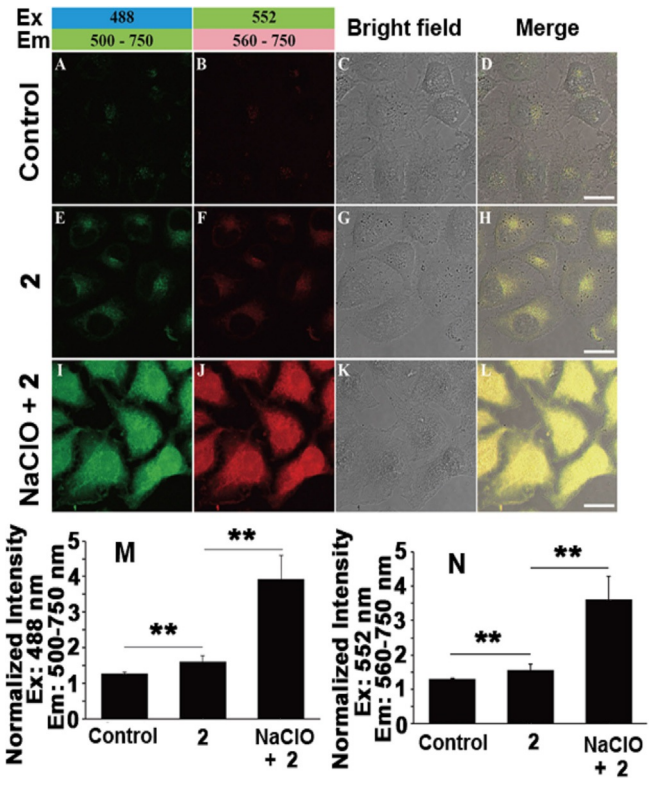

Figure 8. HeLa cells treated with probe **2** and NaClO: A–D) control, E–H) cells treated with probe **2** (12.5 μM) for 2 h at 37 °C, and I–L) cells treated with NaClO for 1 h and then incubated with probe **2** (12.5 μM) for 2 h at 37 °C. The imaging conditions are shown. Scale bar, 20 μm. (M-N) Quantification of the normalized fluorescent intensity of probe **2** in living HeLa cells. Images were collected with excitation at 488 nm and emission at 500–750 nm (M) and with excitation at 552 nm and emission at 560–750 nm (N).

2.4.2. Dual Emission Peaks of Probe 2 in HeLa Cells

Probe **2** exhibited dual emission peaks in chemical studies, and we, therefore, investigated this chemical property in living human cells. We imaged double-ClO^--**2**-HeLa cells by exciting probe **2** with a 488 or 552 nm laser, and then collected the emission signal in 50 nm intervals from 500 to 800 nm or 560 to 800 nm, respectively (Figure 9A–K). The average intensity in each cell across the spectrum was analyzed. The probe **2** emission peak was located at 560–600 nm with 488 nm excitation and at 600–650 nm with 552 nm excitation. However, the emission intensity when excited at 488 nm was significantly higher than when excited at 552 nm (Figure 9L,M). We concluded that probe **2** exhibited chemical properties in vivo that were consistent with those observed in the in vitro studies.

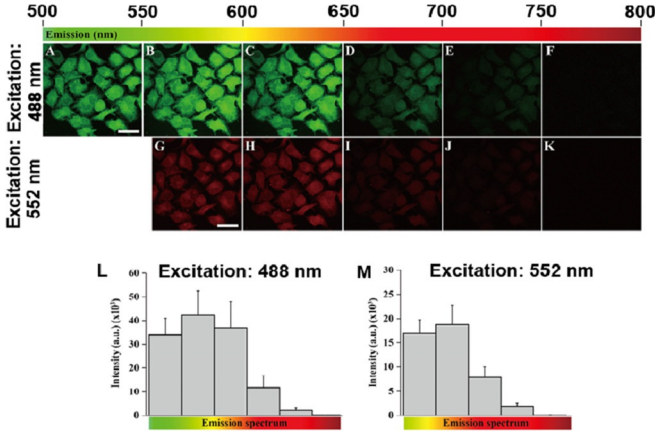

Figure 9. Dual emission peaks in NaClO-**2**-labeled HeLa cells. HeLa cells were treated with NaClO for 1 h and then incubated with probe **2** (12.5 μM) for 2 h at 37 °C. The fluorescence images of the HeLa cells were captured with 488 nm excitation (A–F) and 552 nm excitation (G–K) with different emission wavelengths collected as indicated. The fluorescence intensities were quantified by using ImageJ software. Scale bar, 40 μm.

3. Conclusions

We successfully synthesized probe **1**, which contains only one spirolactone group, and confirmed its structure by using X-ray crystallography. As a novel rhodol-based fluorescence probe, **1** showed excellent selectivity and high sensitivity towards Hg^{2+}, and the spirolactone ring was observed to open in acid conditions because of its $-NEt_2$ group. Probe **2** was designed and

synthesized by functionalizing **1** with a phenyl isothiocyanate group and was found to exhibit good functionality at physiological pH as well as excellent selectivity for HClO. The sensing mechanism of probe **2** involves the cyclization of rhodamine–thiosemicarbazide, which, in the presence of HClO, forms rhodamine–oxadiazole. Confocal microscopy images of HeLa cells incubated with probe **2** showed enhanced fluorescence intensity with HClO, thus demonstrating the potential of probe **2** in further applications in in vivo HClO detection.

Acknowledgements

K.M.C.W. acknowledges receipt of the "Young Thousand Talents Program" award and the start-up fund administrated by Southern University of Science and Technology. This project was also supported by Shenzhen Science and Technology Innovation Commission (Grant Nos. JCYJ20150630145302245 and JCYJ20170307110203786) and National Natural Science Foundation of China (Grant no. 21471074). Y.C.T, H.L, and G.G thank the support by Guangdong Provincial Key Laboratory of Cell Microenvironment and Disease Research (Grant No. 2017B030301018), Shenzhen Key Laboratory of Cell Microenvironment (Grant No. ZDSYS20140509142721429), National Natural Science Foundation of China (Grant No. 31671409) and Shenzhen Science and Technology Innovation Commission (Grant Nos. JCYJ20150529152146477 and JCYJ20170307105005654).

Conflict of Interest

The authors declare no conflict of interest.

Keywords: chemosensor · fluorescence · hypochlorous acid · mercury · rhodol

[1] X. Chen, X. Meng, S. Wang, Y. Cai, Y. Wu, Y. Feng, M. Zhu, Q. Guo, *Dalton Trans.* **2013**, *42*, 14819.

[2] a) J. Fan, M. Hu, P. Zhan, Z. Peng, *Chem. Soc. Rev.* **2013**, *42*, 29; b) X. Chen, Y. Zhou, X. Peng, J. Yoon, *Chem. Soc. Rev.* **2010**, *39*, 2120; c) Z. Xu, J. Yoon, D. R. Spring, *Chem. Soc. Rev.* **2010**, *39*, 1996; d) Z. Liu, W. He, Z. Guo, *Chem. Soc. Rev.* **2013**, *42*, 1568; e) C. Streu, E. Meggers, *Angew. Chem. Int. Ed.* **2006**, *45*, 5645; *Angew. Chem.* **2006**, *118*, 5773; f) M. Schäferling, *Angew. Chem. Int. Ed.* **2012**, *51*, 3532; *Angew. Chem.* **2012**, *124*, 3590.

[3] J. P. Henderson, J. Byun, J. W. Heinecke, *J. Biol. Chem.* **1999**, *274*, 33440.

[4] a) H. Zheng, Z.-H. Qian, L. Xu, F.-F. Yuan, L.-D. Lan, J.-G. Xu, *Org. Lett.* **2006**, *8*, 859; b) J.-S. Wu, I.-C. Hwang, K. S. Kim, J. S. Kim, *Org. Lett.* **2007**, *9*, 907; c) D. Wu, W. Huang, C. Duan, Z. Lin, Q. Meng, *Inorg. Chem.* **2007**, *46*, 1538; d) M. Suresh, A. Shrivastav, S. Mishra, E. Suresh, A. Das, *Org. Lett.* **2008**, *10*, 3013; e) X. Zhang, Y. Xiao, X. Qian, *Angew. Chem. Int. Ed.* **2008**, *47*, 8025; *Angew. Chem.* **2008**, *120*, 8145; f) H. Yu, Y. Xiao, H. Guo, X. Qian, *Chem. Eur. J.* **2011**, *17*, 3179.

[5] B. Mainnemare, A. Mégarbane, A. Souidan, I. L. C. Daniel, J. Chapple, *Dent. Res.* **2004**, *83*, 823.

[6] O Ordeig, R. Mas, J. Gonzalo, *Electroanalysis* **2005**, *17*, 1641.

[7] P. Soldatkin, D. V. Gorchkov, C. Martelet, *Sens. Actuators B* **1997**, *43*, 99.

[8] N. O. Soto, B. Horstkotte, J. G. March, P. L. L. de Alba, L. L. Martinez, V. C. Martin, *Anal. Chim. Acta* **2008**, *611*, 182.

[9] J. Ballesta Claver, M. C. Valencia Mirón, L. F. Capitán-Vallvey, *Anal. Chim. Acta* **2004**, *522*, 267.

[10] a) X. Chen, X. Tian, I. Shin, J. Yoon, *Chem. Soc. Rev.* **2011**, *40*, 4783; b) T. Kim, S. Park, Y. Choi, Y. Kim, *Chem. Asian J.* **2011**, *6*, 1358; c) J. Shepherd, S. A. Hilderbrand, P. Waterman, J. W. Heinecke, R. Weissleder, P. Libby, *Chem. Bio.* **2007**, *14*, 1221; d) X. Chen, X. Wang, S. Wang, W. Shi, K. Wang, H. Ma, *Chem. Eur. J.* **2008**, *14*, 4719; e) J. Shi, Q. Li, X. Zhang, M. Peng, J. Qin, Z. Li, *Sens. Actuators B* **2010**, *145*, 583.

[11] a) S. Goswami, A. Manna, S. Paul, C. K. Quah, H.-K. Fun, *Chem. Commun.* **2013**, *49*, 11656; b) S. Goswami, A. K. Das, A. Manna, A. K. Maity, P. Saha, C. K. Quah, H.-K. Fun, H. A. Abdel-Aziz, *Anal. Chem.* **2014**, *86*, 6315; c) A. Manna, D. Sarkar, S. Goswami, C. K. Quah, H.-K. Fun, *RSC Adv.* **2016**, *6*, 57417; d) A. Manna, S. Goswami, *New J. Chem.* **2015**, *39*, 4424.

[12] Q. P. Zhu, Z. J. Li, Y. H. Hu, B. Li, L. H. Huang, C. J. Wang, S. K. Liu, H. Q. Liao, *J. Fluoresc.* **2012**, *22*, 1201; https://doi.org/10.1007/s10895-012-1067-8.

[13] M. D. Pluth, E. Tomat, S. J. Lippard, *Ann. Rev. Biochem.* **2011**, *80*, 333.

[14] C. Wang, K. M. C. Wong, *Inorg. Chem.* **2013**, *52*, 13432.

[15] a) T. Peng, D. Yang, *Org. Lett.* **2010**, *12*, 496; b) S. C. Burdette, S. J. Lippard, *Inorg. Chem.* **2002**, *41*, 6816; c) H. Komatsu, Y. Shindo, K. Oka, J. P. Hill, K. Ariga, *Angew. Chem. Int. Ed.* **2014**, *53*, 3993; *Angew. Chem.* **2014**, *126*, 4074; d) B. C. Dickinson, C. J. Chang, *J. Am. Chem. Soc.* **2008**, *130*, 9638; e) B. C. Dickinson, C. Huynh, C. J. Chang, *J. Am. Chem. Soc.* **2010**, *132*, 5906; f) M. Kamiya, D. Asanuma, E. Kuranaga, A. Takeishi, M. Sakabe, M. Miura, T. Nagano, Y. Urano, *J. Am. Chem. Soc.* **2011**, *133*, 12960; g) X.-F. Yang, Q. Huang, Y. Zhong, Z. Li, H. Li, M. Lowry, J. O. Escobedo, R. M. Strongin, *Chem. Sci.* **2014**, *5*, 2177.

[16] L. Li, Wang, C. J. Wu, Y. C. Tse, Y. P. Cai, *Inorg. Chem.* **2016**, *55*, 205.

[17] a) C. Wang, K. M. C. Wong, *Inorg. Chem.* **2011**, *50*, 5333; b) C. Wang, H. C. Lam, N. Zhu, K. M. C. Wong, *Dalton Trans.* **2015**, *44*, 15250; c) K. M. C. Wong, C. Wang, H. C. Lam, N. Zhu, *Polyhedron* **2015**, *86*, 133.

[18] R. W. Sabnis, *Handbook of acid-base indicators*, CRC Press, Baco Raton, **2008**.

[19] Y. Koide, Y, Urano, S. Kenmoku, H. Komija, T. Nagano, *J. Am. Chem. Soc.* **2007**, *129*, 10324.

Received: September 21, 2017
Version of record online December 6, 2017

